Journal of Hazardous Materials 399 (2020) 122949

Contents lists available at ScienceDirect

Journal of Hazardous Materials

journal homepage: www.elsevier.com/locate/jhazmat

Facile and scalable synthesis of silicon nanowires from waste rice husk silica by the molten salt process

Jong-Hyeok Choi[a,1], Hyun-Kyung Kim[b,1], En-Mei Jin[a], Myung Won Seo[c], Jung Sang Cho[d], R. Vasant Kumar[e], Sang Mun Jeong[a,*]

[a] Department of Chemical Engineering, Chungbuk National University, 1 Chungdea-ro, Seowon-gu, Choengju 28644, Republic of Korea
[b] Department of Materials Science and Engineering, Kangwon National University, Chuncheon 24341, Republic of Korea
[c] Clean Fuel Laboratory, Korea Institute of Energy Research (KIER), 152 Gajeong-ro, Yuseong-gu, Daejeon 34129, Republic of Korea
[d] Department of Engineering Chemistry, Chungbuk National University, 1 Chungdea-ro, Seowon-gu, Cheongju 28644, Republic of Korea
[e] Department of Materials Science and Metallurgy, University of Cambridge, 27 Charles Babbage Rd, Cambridge CB3 0FS, United Kingdom

GRAPHICAL ABSTRACT

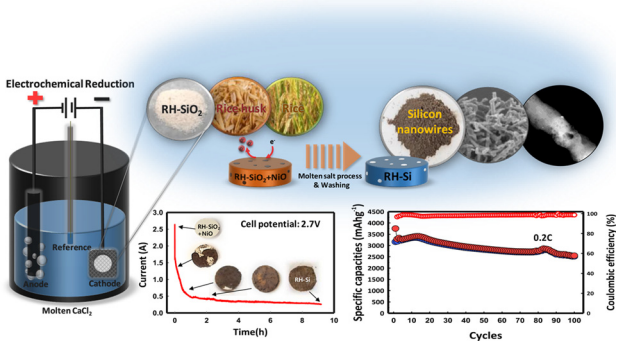

ARTICLE INFO

Editor: Markus Hecker

Keywords:
Waste biofuel
Energy storage materials
Rice husk

ABSTRACT

Designing nanostructured silicon, such as in the form of nanoparticles, wires, and porous structures, for high-performance Li-ion electrodes, has progressed significantly. These approaches have largely overcome the capacity fading of silicon electrodes from volume expansion during lithiation/de-lithiation. However, they involve high costs, complex processes, and hazardous precursors. Herein, we propose an electrochemical fabrication of silicon nanowires from waste rice husks via a molten salt process based on electrodeoxidation. The addition of NiO as an electric conductor improved the production efficiency and created pores in the nanowires after washing. The electrically produced high-purity silicon yielded high capacity, and the nanowires provided sufficient free volume to accommodate silicon electrode expansion, resulting in improved cycle life. The converted silicon nanowires from the molten salt process will help develop sustainable energy storage materials.

Abbreviations: RH, rice husk; LIBs, lithium-ion batteries; VLS, vapor-liquid-solid; CVD, chemical vapor deposition; SFLS, supercritical fluid-liquid-solid; PVA, Polyvinyl alcohol; DC, direct current; CV, cyclic voltammetry; MCE, metallic cavity electrode; FE-SEM, field emission-scanning electron microscopy; EDS, energy-dispersive X-ray spectroscopy; HR-TEM, high-resolution transmission electron microscopy; XPS, X-ray photoelectron spectroscopy; XRD, X-ray diffraction; GCD, Galvanostatic charge-discharge; SAED, selected area electron diffraction

* Corresponding author.
E-mail address: smjeong@chungbuk.ac.kr (S.M. Jeong).
[1] These authors (J.H.C. and H.K.K.) contributed equally to this work.

https://doi.org/10.1016/j.jhazmat.2020.122949
Received 22 March 2020; Received in revised form 20 April 2020; Accepted 11 May 2020
Available online 16 May 2020
0304-3894/ © 2020 Elsevier B.V. All rights reserved.

1. Introduction

The research community is engaged in significant effort toward solving environmental and energy shortage issues caused by rapid industrialization; in this regard, as a renewable energy resource, biomass has attracted increasing interest. Rice husk (RH) is a byproduct of rice, the second most highly cultivated crop species worldwide (7.7×10^8 tons/year) (Food and Agriculture Organization FAO (2018), and typically constitutes 20–22 % of rice production (Bansal et al., 2006). Surprisingly, waste RH contains a relatively high content of silica compounds, averaging at approximately 10.6 % (Bansal et al., 2006). RH silica (RH-SiO_2) is obtained from RH by thermal treatment (400–900 ˚C), and leaching (Real et al., 1996; Chakraverty et al., 1988; Ghosh et al., 2013; Cho et al., 2016; Kumproa et al., 2012). Since biological silica derived from the biosilification of organisms has a complicated and hierarchical nanostructured framework (Ehrlich et al., 2010), it has a wide range of applications (Adam et al., 2012; Athinarayanan et al., 2015). In addition, crystalline silicon (Si), which plays an essential role in the fabrication of numerous applications, can be produced by the reduction of biogenic silica (Shah et al., 1999; Shen et al., 2017). Therefore, RH has potential as a low-cost precursor for producing green and high-value materials requiring Si for practical applications.

Specifically, Si is a promising anode material with a high theoretical specific capacity and a low lithiation reaction voltage plateau (vs. Li/Li^+) (Kasavajjula et al., 2007; Chan et al., 2008), and is commonly used in lithium-ion batteries (LIBs). However, Si typically suffers from irreversible capacity fading during cycling from three distinct causes: (1) pulverization of Si particles due to significant volume expansion during lithiation and disintegration of the composite electrode architecture; (2) formation of an unstable solid electrolyte interphase (Luo et al., 2017; Xu et al., 2015); and (3) relatively low intrinsic electronic and ionic conductivities (Luo et al., 2017; Casimir et al., 2016). To address these issues, several strategies have been reported, such as the use of nanostructured Si (Kim et al., 2010; Park et al., 2009; Liu et al., 2013), Si/C composites (Cui et al., 2016; Liu et al., 2012; Luo et al., 2012), Si alloys (Zhou et al., 2010), and thin film (Kim et al., 2003), all of which help to prevent the capacity fading of Si-based systems.

In particular, for the nanostructural design of Si with various morphologies, Si nanowires (Si-NWs), Si nanoparticles, and porous structures are promising as high-performance anode materials (Wu and Cui, 2012). Notably, NWs have several advantages, including: (1) sufficient empty space between adjacent NWs to accommodate Si volume changes upon charging and discharging, (2) effective electron transport along each NW, and (3) facile strain relaxation with increasing wire diameter and length, without cracking or breakage (Chan et al., 2008; Wu et al., 2012; Chan et al., 2010). Taking advantage of these effects, several studies have demonstrated enhanced cycle lives using methods such as vapor-liquid-solid (VLS) (Chan et al., 2008), chemical vapor deposition (CVD) (Nguyen et al., 2011), and supercritical fluid-liquid-solid (SFLS) processes (Chan et al., 2010; Chockla et al., 2011), by directly coating stainless-steel current collectors to ensure good contact. However, despite successful demonstrations of Si-NW electrodes, there remain fundamental barriers toward their large-scale implementation in LIBs. These methods involve high manufacturing costs (VLS) (Liu et a., 2011), potentially hazardous precursors (CVD) (Nguyen et al., 2011), and low yields (SFLS) (Chan et al., 2010). Overall, it is highly desirable to fabricate nanostructured Si in an affordable and non-hazardous manner based on a sustainable resource.

Herein, we demonstrate a molten salt electrolysis method for the fabrication of Si-NWs for LIB anode materials from RH-derived SiO_2. Crystalline Si-NWs were prepared through application of the FFC Cambridge process (Mohandas and Fray, 2004), a simple approach for the high-purity extraction of metals from solid oxides via molten salt electrolysis that is known to be energy-saving and environmentally friendly. The prepared Si-NWs resolve many of the critical issues for effective Si-based battery operation and exhibit excellent electrochemical performance as LIB anodes, suggesting that RH-SiO_2 is a large-scale resource for high-capacity LIB applications.

2. Methods

2.1. Preparing Si-NWs from RH

Amorphous SiO_2 was leached from RH via a conventional leaching and thermal process (Cho et al., 2016). To produce pellet-type RH-SiO_2 + nickel oxide (NiO), RH-SiO_2 and NiO (99 % purity, Alfa Aesar) were mixed together in a mortar (atomic ratio SiO_2:NiO = 20:1) with ethanol (95.0 % purity, SAMCHUN, South Korea). Polyvinyl alcohol (PVA, M_w 89,000–98,000, 99 + % hydrolyzed, Aldrich) and zinc stearate (technical grade, Aldrich) were added as binders, which were dried at 80 ˚C for 24 h. The dried powders (approximately 1.0 g) were pressed at 100 bar in a cylindrical mold (∅ = 13 mm), followed by sintering at 1200 ˚C in air for 5 h to prepare a solid pellet for electrodeoxidation. An Al_2O_3 crucible (99 % purity, ∅ = 80 mm) charged with 500 g of $CaCl_2$ (95.0 + %, Junsei, Japan) was set inside a stainless-steel vessel and heated to 850 ˚C in a dry Ar atmosphere. The $CaCl_2$ salt was pre-dried at 550 ˚C for 1 d. An RH-SiO_2 + NiO pellet was wrapped in nickel mesh (20 mesh woven from 0.18-mm-diameter wire, Alfa Aesar), which was used as a working electrode by fastening it to a stainless-steel rod with nickel wire (∅ = 0.5 mm, Alfa Aesar). The nickel mesh and wire acted as the current lead, and a graphite rod was used as the anode. A hole (4 mm) was drilled through a graphite rod (99 %, Alfa Aesar) to connect it to the stainless-steel rod. The reference electrode was a Ag/AgCl electrode in which a silver wire (99.99 %, ∅ = 0.5 mm, Aldrich) was immersed in a $CaCl_2$ melt containing 1 M AgCl (99.5 %, SAMCHUN, South Korea) in a mullite tube. The electrodeoxidation of the RH-SiO_2 + NiO pellet was performed by applying a cell voltage in the 2.7–2.9 V range for 0–10 h, which was controlled with a direct current (DC) power supply (E3633A, Agilent). The cathodic potential (vs. Ag/AgCl) was continuously monitored during electrolysis with a multi-meter (34,401A, Agilent). After electrolysis, the cathode product was rinsed with deionized water and dried in a vacuum oven. The obtained Si powder was soaked in a 0.1 M HCl (SAMCHUN, South Korea) solution for 1 d to remove impurities, and then leached in 2% hydrofluoric acid (Alfa Aesar) for 12 h with vigorous stirring to ensure the removal of any unreduced SiO_2. For cyclic voltammetry (CV), Mo wire (99.95 % purity, Alfa Aesar) was used to fabricate a metallic cavity electrode (MCE) with two pin holes (∅ = 0.5 mm). RH-SiO_2 + NiO powder was placed into the holes of the MCE as the working electrode. The cell was controlled by a potentiostat (Autolab, PGSTAT362 N) at a scan rate of 100 mV/s.

2.2. Characterizing RH-SiO_2 and Si-NWs

Electron microscopy was carried out by field emission-scanning electron microscopy (FE-SEM, ULTRA PLUS-FESEM), energy dispersive X-ray spectroscopy (EDS, FlatQUAD), and high-resolution transmission electron microscopy (TEM, HRTEM; 300 kV Tecnai G2 F30 S-Twin field emission gun). The crystal structures were determined by X-ray diffraction (XRD; AXS D8 Discover with GADDS, Bruker) with Cu-K α radiation (wavelength = 0.54 Å). The chemical compositions of all sample surfaces were analyzed by Raman spectroscopy (LabRam HR, Horiba Jobin Yvon) and X-ray photoelectron spectroscopy (XPS; PHI Quantera-II, Ulvac-PHI).

2.3. Battery testing the Si-NWs

For the application of the anode active material, slurries were prepared by dissolving 55 wt% Si-NWs, 35 wt% super P (99 + %, Alfa Aesar), and 10 wt% poly(acrylic) acid (M_w ~ 100,000, 35 wt% in H_2O, Aldrich) in distilled water. The slurries were cast onto a copper current collector by a doctor blade technique. Si powder (99.5 %, ~325 mesh,

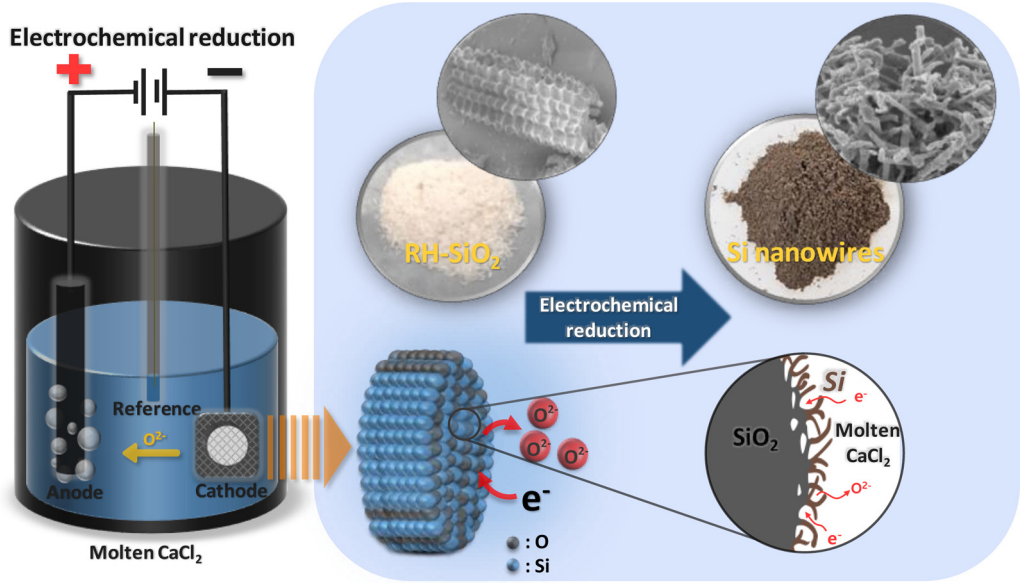

Fig. 1. Schematic illustration of electrochemical fabrication of silicon nanowires (Si-NWs) from rice husk-derived silica (RH-SiO_2).

Alfa Aesar) was used for comparison, for which slurries were prepared with the same composition. The active materials were loaded at 0.6 mg/cm^2. After drying at 80 °C in air, the electrode was pressed to 80 % of its original thickness by a roll-press (MSK-HRP-01, MTI) and then vacuum dried at 120 °C. Each electrode was in a CR-2032-type coin cell with Li metal as the counter electrode. The electrolyte was 1.15 M $LiPF_6$ in a mixture of ethylene carbonate and dimethyl carbonate at a 3:7 vol ratio with 10 % fluorinated ethylene carbonate. A microporous membrane (Celgard 2400) was used as a separator. The coin cells were assembled in an Ar-filled glove box (99.99 % purity). Galvanostatic charge-discharge (GCD) testing (WBCS3000 L, Wonatech) was conducted for 100 cycles in the 0.01–1.5 V (vs. Li^+/Li) range at a 0.2 C rate (1 C = 4200 mA h/g), where the first three cycles were performed at a 0.05 C rate, and rate capability testing was conducted at 0.1, 0.2, 0.5, 1.0, and 2.0 C rates.

3. Results and discussion

Fig. 1 shows a schematic illustration of the electrodeoxidation process for Si-NWs from a RH-SiO_2 + NiO pellet at 850 °C. Pellets fabricated at various weights (0.3–1 g) are shown in Figure S1 (Supplementary Material), which demonstrate the scalability of the molten salt method. Amorphous RH-SiO_2 + NiO powders were sintered at a high temperature after being compressed to undergo a phase transition to crystalline SiO_2, which can be observed in the XRD pattern shown in Figure S2. The broad XRD pattern of the amorphous RH-SiO_2 powder changes to that of a perfect crystal structure after sintering; the strongly compressed pellets prevent decrepitation of the prepared pellets in the molten salts. The RH-SiO_2 functions as the cathode in the electrolytic cell containing the molten salt electrolyte, typically $CaCl_2$, and a graphite anode. Following the pre-electrolysis of the molten $CaCl_2$ at 850 °C, the cell is polarized such that the cathode reaches a negative potential sufficient to ionize oxygen in the electrode (Fray and Schwandt, 2017; Chen et al., 2000). NiO was added to the starting material used as the cathode to enhance the reduction efficiency of the insulating RH-SiO_2. Ni formation by co-reduction of the SiO_2 + NiO system increases the electrical conductivity of the cathode during electrode-deoxidation, making it more effective (Ji et al., 2013). Eventually, oxygen is gradually released from RH-SiO_2 into the electrolyte, and the Si-NW growth mechanism is proposed to operate as follows (Xiao et al., 2006; Yasuda et al., 2005a): (1) Upon immersing the RH-SiO_2 + NiO contacting electrode into the molten $CaCl_2$, the Ni from NiO initially serves as the conducting material; SiO_2 near the Ni is converted into Si through the removal of oxygen with only a limited amount of SiO_2 reduced to form nanoscale Si nuclei, which are separately located on the $SiO_2/CaCl_2$ interface. These Si nuclei immediately collide with nearest-neighbor SiO_2 in terminated channels from the molten $CaCl_2$ that penetrate into the SiO_2. (2) Because the formed Si nuclei are highly conductive at a high temperature, they behave as a new conducting material; hence, subsequent reduction is limited to the newly formed Si nuclei/$SiO_2/CaCl_2$ three-phase interface, resulting in wire-type Si. The prepared Si-NWs form with the ability to alleviate volume changes in Si-based anode materials.

From a thermodynamic perspective, during the molten salt process the standard Gibbs free energies for reducing SiO_2 ($SiO_2 \rightarrow Si^{4+} + 2O^{2-}$) and NiO ($NiO \rightarrow Ni^+ + 1/2O^{2-}$) at 850 °C are 708.9 kJ/mol and 137.9 kJ/mol, respectively. This difference is clearly evident in the CV results shown in Fig. 2 (a) in the -2.0–0.9 V (vs. Ag/AgCl) potential window. The CV curve (black solid line) of the Mo MCE is compared with those of the NiO (red solid line) and SiO_2 + NiO (blue solid line) electrodes. The cathodic current increases sharply at -1.8 V, and an anodic current is observed in the reverse scan, which contributes to the deposition and dissolution of calcium in the Mo MCE. The NiO shows a cathodic current beginning at 0.028 V, with the highest peak observed at -0.25 V due to its high electrical conductance and low standard Gibbs free energy (Lee et al., 2016). For RH-SiO_2 + NiO, the cathodic current occurs at -0.028 V and is followed by a significant increase at around -1.34 V; the initial current is almost identical to the potential of the maximum peak at -0.028 V due to NiO reduction, and a large current is observed at around -1.34 V for the Ni metal located around SiO_2. As a result, Ni metal improves the electrical conductivity and assists in the quick reduction of the electrical insulator (SiO_2). This process reduces the reduction time and energy by increasing the efficiency of the electrolytic reduction reaction in the molten salt, thereby achieving the rapid reduction of SiO_2 on the gram scale.

Fig. 2 (b) shows the cathodic potential per cell voltage plots during the electrolytic reduction; the potential for calcium deposition is approximately -1.8 V as shown in Fig. 2 (a), and the appropriate cell voltage is 2.7 V (solid black line) (Yasuda et al., 2005b). These results demonstrate the reduction behavior of the RH-SiO_2 + NiO pellet with the time-current plot per charge amount applied at 2.7 V during constant electrical potential electrolysis. The RH-SiO_2 + NiO pellet has a higher current than that of RH-SiO_2, which contributes to increased pellet conductivity due to early formation of Ni metal during reduction

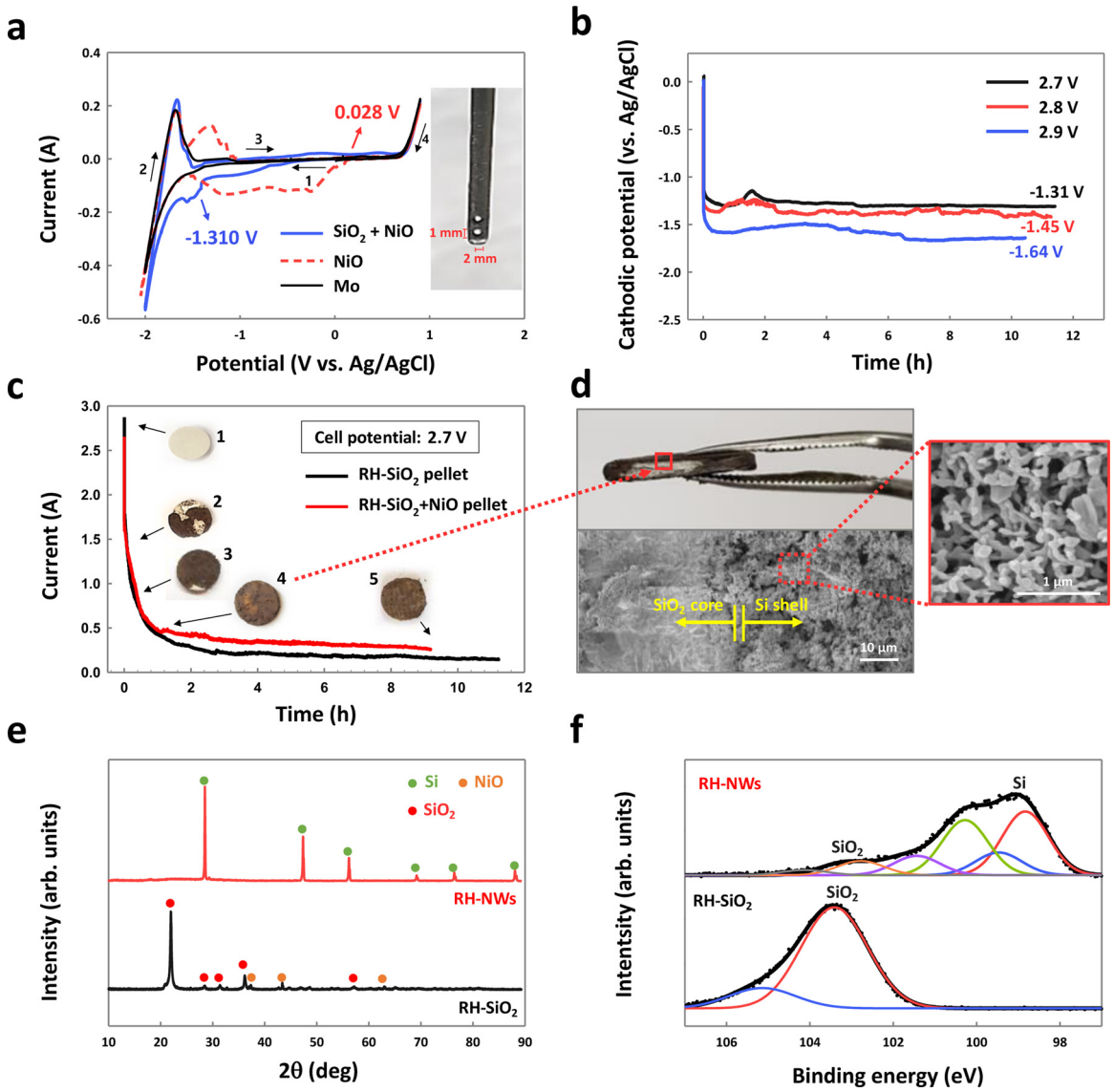

Fig. 2. Electrochemical reduction behavior and structural analysis of RH-SiO_2 + NiO pellet and prepared Si-NWs. (a) Cyclic voltammograms of bare Mo MCE, RH-SiO_2 + NiO, and NiO electrodes (at -2.0–0.9 V) and (b) cathode potential-time plots of various cell potentials. (c) Time-current plots of RH-SiO_2 and RH-SiO_2 + NiO pellets with photographs of reduced samples with various supplied charges of 0%, 10 %, 20 %, 50 %, and 400 % (numbers 1–5) of the theoretical charge at 2.7 V. (d) Photographic image of sample 4 and a magnified scanning electron microscopy image of the marked region. (e) X-ray diffraction patterns and (f) X-ray photoelectron spectra of RH-SiO_2 and the prepared Si nanowires.

as shown in Figure S3. Additionally, we compared and observed the appearance of the pellet before and after the electrolytic reduction of the RH-SiO_2 + NiO/RH-SiO_2 hybrid pellets and RH-SiO_2 pellets under the same condition for the same duration. The reduction rate of the RH-SiO_2 + NiO/RH-SiO_2 hybrid pellets was very rapid compared with those of the RH-SiO_2 pellets as shown in Figure S4. Consequently, the generation of Ni during the reduction process increased the electrical conductivity and reduction efficiency. The reduction process generally starts from the surface and proceeds to the core of the pellet, as shown in Fig. 2 (c) and (d); this mechanism forms the conductor/insulator/electrolyte three-phase interface and finally leads to the successful preparation of wire-type Si (Nohira et al., 2003). Figure S5 shows the XRD patterns of the samples, indicating the deoxidation process of RH-SiO_2 in Fig. 2 (c). The initial 0% (vs. theoretical electric charge of SiO_2) charged sample has the same XRD pattern as that of the prepared RH-SiO_2 + NiO pellet. For the 10 % charged sample, crystalline Si peaks appear in the XRD pattern, which increase in intensity as the electrolytic reduction proceeds, which may indicate that reduction repeatedly occurs at a constant potential over a longer period. Finally, the XRD pattern of the 400 % charged sample displays no SiO_2 peak, which shows that the RH-SiO_2 + NiO pellet has been completely reduced to pure Si and Ni metals. Furthermore, the XRD peaks of the 400 % charged sample are divided, which are attributable to reduced Ni and Si reacting with each other to generate $NiSi_2$ (JCPDS No. 04-006-9129) (Fang et al., 2015). After acid treatment, the XRD spectra verify the pure phase of crystalline Si (JCPDS No. 27-1402) as shown in Fig. 2 (e). XPS spectra were acquired to investigate the surface contents of the RH-SiO_2 and prepared Si-NWs. In Fig. 2 (f), the peaks at approximately at 98.8 and 99.4 eV are attributed to Si, and the peak at 103.5 eV is assigned to Si^{4+}, suggesting the existence of small amounts of amorphous SiO_2 (Gauthier et al., 2013), which is typically formed during exposure of Si to the atmosphere. The Raman spectrum is consistent with the XPS results, as shown in Figure S6. RH-SiO_2 exhibits three Raman peaks at 486, 980, and 1080 cm^{-1} that correspond to a Si-O-Si symmetric stretching vibration, a Si-O stretching vibration, and movement of oxygen within the silicon lattice, respectively. However, the Raman

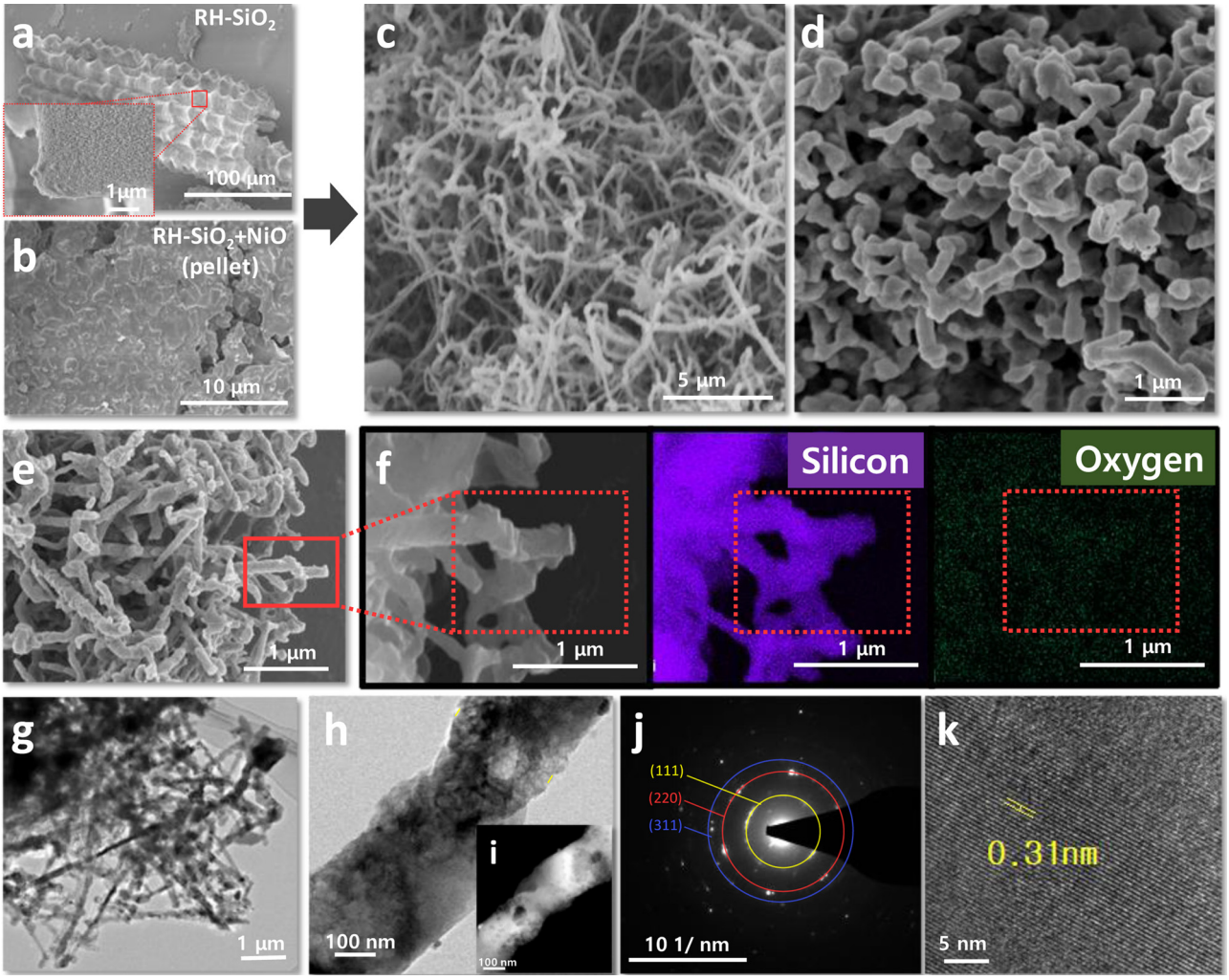

Fig. 3. Morphological analysis of silicon nanowires by electrochemical reduction. Scanning electron micrographs of (a) RH-SiO_2 powder, (b) RH-SiO_2 + NiO pellet, (c) and (d) nanowires after electrochemical reduction, and (e) prepared Si nanowires after acid treatment. (f) Scanning electron microscopy–energy-dispersive X-ray spectroscopy maps of Si and O. (g) and (h) Transmission electron micrographs, (i) Scanning transmission electron micrograph, (j) Selected area electron diffraction pattern and (k) High-resolution transmission electron micrographs of prepared Si nanowires.

spectrum of the prepared Si-NWs only shows a sharp peak at 518 cm^{-1} due to crystalline Si, suggesting that the RH-SiO_2 had been converted into pure Si devoid of Si-O-Si or Si-O bonds (Choi et al., 2018).

The morphology and crystalline quality of the Si-NWs produced before and after electrolysis of the RH-SiO_2 pellet were investigated using SEM, HRTEM, and scanning TEM (STEM). Fig. 3 (a) and (b) shows the SEM images of the RH-SiO_2 before and after the molten salt process involving the RH-SiO_2 + NiO pellet. The images in Fig. 3 (a) clearly confirm the unique three-dimensional (3D) hierarchical porous structure of RH-SiO_2 at low and high magnifications. Furthermore, NiO is well distributed on the RH-SiO_2 of the prepared RH-SiO_2 + NiO pellet as indicated by the SEM and EDS maps shown in Figure S3. Fig. 3 (c)–(f) shows the SEM images of the prepared Si-NWs after application of a constant potential of 2.7 V for 10 h to a RH-SiO_2 + NiO pellet in $CaCl_2$ molten salt at 850 °C. The reaction begins at the surface of the SiO_2, as discussed above (Nohira et al., 2003), and eventually proceeds to the core of the pellet. After electrolysis of the RH-SiO_2 + NiO pellet, Si and $NiSi_2$ (Fang et al., 2015), have wire-type structures, as shown in Fig. 3 (c) and (d). The structure was well maintained even after washing with distilled water and treating with acid to remove Ni, and the images clearly confirmed the NW shape of the pure Si, as shown in Fig. 3 (e) and (f). These results clearly indicate that the Si has a wire-type nanostructure with a wire diameter of ~300 nm and length > 1 μm, which is indeed consistent with the various scaled SEM and TEM images shown in Figure S7. Additionally, the high-purity wire-type Si has an oxygen concentration of only 7100 ppm according to the EDS results shown in Figure S8. The prepared Si-NWs also show similar TEM and STEM results (Fig. 3 (g), (h), and S7). Moreover, as shown in Fig. 3 (i) and S9, small nanopores were randomly generated on the wires due to the deoxidation and acid treatment used to remove the Ni. These pores are desirable as they improve ionic conductivity and reduce the volume expansion of silicon during charging and discharging as an anode material for use in LIBs. Additionally, we compared the structural properties and electrochemical performance of Si-NW and Si, which were obtained through electrolytic reduction processes using RH and commercial SiO_2, respectively, as the starting materials as shown in Figure S10. The commercial SiO_2 was composed of simple particle structures, which produced uneven particles with hundreds of nanometers of wires clustered together after the completion of the electrolytic reduction process. Furthermore, the HRTEM image (Fig. 3 (j)) also shows lattice fringes corresponding to the Si (111), (220), and (311) planes, highlighting the crystalline character of the pure Si-NWs. The crystalline structure was also confirmed by selected-area electron diffraction (SAED) (Fig. 3 (k)), which exhibits a diffraction ring corresponding to the Si (111) plane.

The Si-NWs were electrochemically tested primarily in GCD experiments. The GCD curves for the Si-NW anode are shown in Fig. 4 (a) for 100 cycles, from which the specific capacity was calculated based on

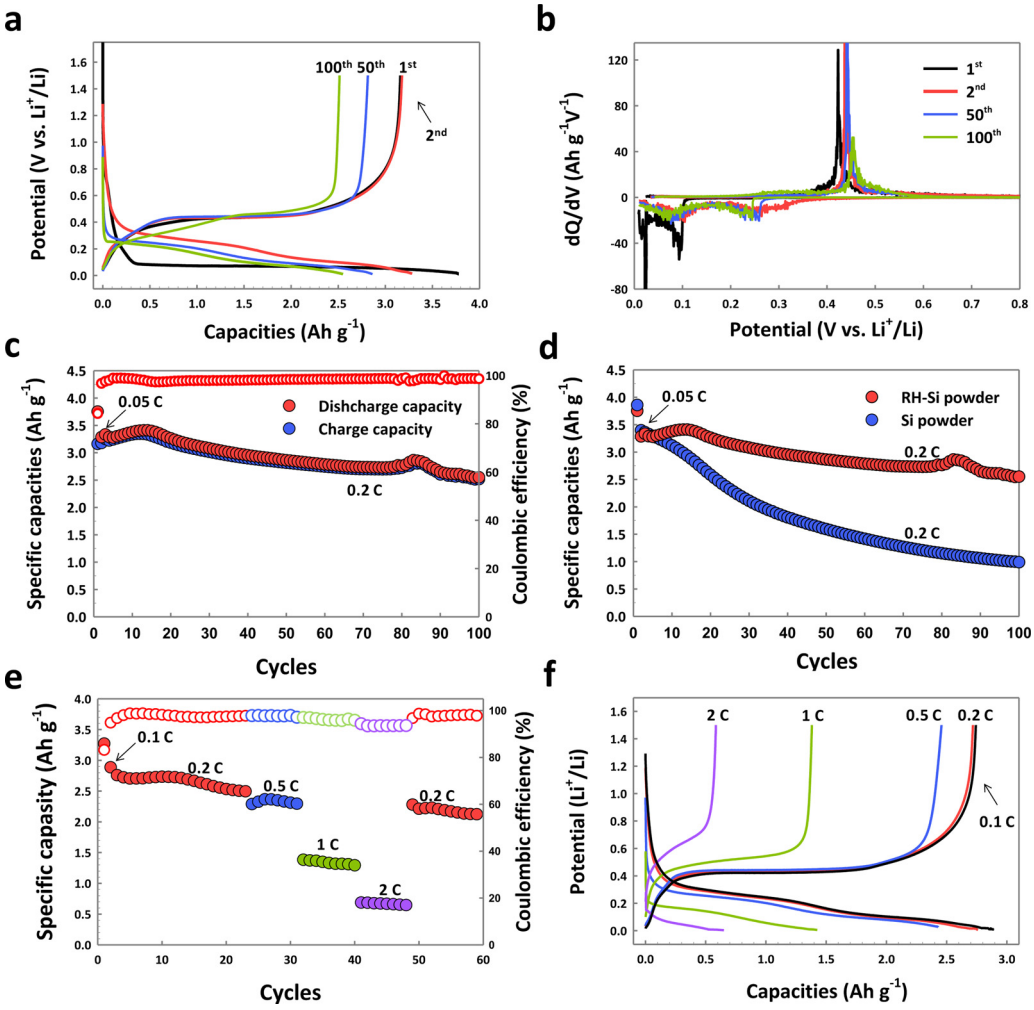

Fig. 4. Electrochemical characterization of the silicon nanowires. (a) Charge–discharge curves and (b) d*Q*/d*V* profiles of the prepared silicon nanowire electrode in the potential range of 0.01–1.5 V vs. Li^+/Li. (c) Lithiation/de-lithiation capacity and Coulombic efficiency of the prepared silicon nanowire electrode and (d) comparison with a commercially prepared silicon powder electrode (first three cycles tested at a 0.05 C rate). (e) Rate performance (first two cycles tested at a 0.1 C rate) and (f) charge-discharge curves for the prepared silicon nanowire electrode at various current densities.

the Si mass in the electrode. The Si-NW anode exhibits a characteristic voltage plateau at 0.05 V during the 1st lithiation, which is associated with the Li–Si alloying process and is indicative of the formation of a well-defined (electrochemically active/favorable) Si phase by the molten salt method. The initial lithiation and de-lithiation capacities of the Si-NW anode were found to be 3752 and 3161 mA h/g at a 0.05 C-rate, respectively, corresponding to coulombic efficiencies (CE) > 84 %, which is in good agreement with pure Si-based anodes with Li-alloying mechanisms. In addition, the lithiation/de-lithiation capacities of the Si-NW anode stabilized rapidly at 3177 and 3284 mA h/g at a 0.2 C rate, respectively, during subsequent cycling. This feature is better understood by plotting d*Q*/d*V* as a function of voltage, as shown in Fig. 4 (b). After attaining a characteristic cathodic peak at 0.05 V during the 1st lithiation (attributed to the 1st Li–Si alloying process), the peak positions/intensities were similar for the 2nd, 50th, and 100th cycles, which implies significant electrochemical reversibility. It is noteworthy that this wire-type Si anode exhibits high usability as well as a stable cycling performance (Fig. 4 (c)), and that the capacity remains at ~2550 mA h/g after 100 cycles while exhibiting high/stable CEs of ~99 % during cycling. As shown in Fig. 4 (d), the cycling performance of the prepared Si-NWs is clearly better than that of the commercial Si powder. After 100 cycles, the prepared Si-NWs and commercial Si powder retained 78 % and 29 % of their initial capacities, respectively. Moreover, the wire-type Si also demonstrates a good rate capability as shown in Fig. 4 (e) and (f). For instance, the electrode exhibits second discharge capacities of 2886, 2759, 2327, and 1371 mA h/g at 0.1, 0.2, 0.5, and 1 C rates, respectively, and retains 650 mA h/g even at the fast 2 C rate. In addition, when the current density is reverted to 0.2 C, the capacity of the Si-NW anode stabilizes at 2279 mA h/g, which corresponds to a recovery rate of 91 %. These results confirm that the prepared Si-NWs have several advantages that led to improved cyclability and rate capabilities during charging and discharging: (1) sufficient empty space between adjacent NWs to accommodate Si volume changes during charging and discharging; (2) effective electron transport along the length of each NW; and (3) facile strain relaxation with increasing wire diameter and length without cracking or breakage. Additionally, the TEM image of the Si-NW electrode taken after 40 cycles exhibits a well-maintained interconnected porous structure, as shown in Figure S11, verifying the robust nature of the wire-type silicon nanostructured electrode.

4. Conclusion

The present study demonstrated the growth of crystalline Si-NWs by electrolysis in molten $CaCl_2$ using waste RH-SiO_2 as a starting material. We showed that RH, a major byproduct of rice harvesting, can be used to produce Si-NWs for use in high-capacity LIB anodes. The interconnected 3D hierarchical structure NWs developed through years of

natural evolution for the efficient cultivation of rice can resolve important issues in Si anode operation and enable excellent cycling and power performance; using this approach, enhanced battery performance was achieved. At a 0.2 C rate, ~3284 mA h/g was attained during the 1st cycle, and a long 100-cycle life was achieved with a capacity retention of 78 % and high specific capacity of 2550 mA h/g. These results show that this method can produce nanostructured metals or alloys from other parent oxides. Furthermore, the method is easy to scale up and consequently will lead to an industrial route for the mass production of Si-NWs for LIBs and various other applications.

CRediT author statement

J.-H.C., H.-K.K., and S.M.J. designed the materials and experiments.
J.-H.C. fabricated the materials.
J.-H.C. and H.-K.K. performed electrochemical characterisation.
E.-M.J., M.W.S., and J.S.C. participated in electrochemical evaluations and structural characterisation.
H.-K.K. and J.-H.C. wrote the manuscript.
R.V.K., and S.M.J. reviewed the manuscript.
All authors discussed the results and commented on the manuscript.

Declaration of Competing Interest

The authors declare that they have no known competing financial interests or personal relationships that could have appeared to influence the work reported in this paper.

Acknowledgments

This work was supported by a National Research Foundation of Korea (NRF) grant funded by the Korea government (MSIT) [grant number 2018R1A4A1024691]. We are grateful to Prof. Derek J. Fray of the Department of Materials Science and Metallurgy at University of Cambridge for his contribution in reviewing the manuscript.

Appendix A. Supplementary data

Supplementary material related to this article can be found, in the online version, at doi:https://doi.org/10.1016/j.jhazmat.2020.122949.

References

Adam, F., Appaturi, J.N., Iqbal, A., 2012. The utilization of rice husk silica as a catalyst: review and recent progress. Catal. Today 190, 2–14. https://doi.org/10.1016/j.cattod.2012.04.056.
Athinarayanan, J., Periasamy, V.S., Alhazmi, M.A., Alatiah, K.A., Alshatwi, A.A., 2015. Synthesis of biogenic silica nanoparticles from rice husks for biomedical applications. Ceram. Int. 41, 275–281. https://doi.org/10.1016/j.ceramint.2014.08.069.
Bansal, V., Ahmad, A., Sastry, M., 2006. Fungus-mediated biotransformation of amorphous silica in rice husk to nanocrystalline silica. J. Am. Chem. Soc. 128, 14059–14066. https://doi.org/10.1021/ja062113+.
Casimir, A., Zhang, H., Ogoke, O., Amine, J.C., Lu, J., Wu, G., 2016. Silicon-based anodes for lithium-ion batteries: effectiveness of materials synthesis and electrode preparation. Nano Energy 27, 359–376. https://doi.org/10.1016/j.nanoen.2016.07.023.
Chakraverty, A., Mishra, P., Banerjee, H.D., 1988. Investigation of combustion of raw and acid-leached rice husk for production of pure amorphous white silica. J. Mater. Sci. 23, 21–24. https://doi.org/10.1007/BF01174029.
Chan, C.K., Peng, H., Liu, G., McIlwrath, K., Zhang, X.F., Hugins, R.A., Cui, Y., 2008. High-performance lithium battery anodes using silicon nanowires. Nat. Nanotechnol. 3, 31–35. https://doi.org/10.1038/nnano.2007.411.
Chan, C.K., Patel, R.N., O'Connell, M.J., Korgel, B.A., Cui, Y., 2010. Solution-grown silicon nanowires for lithium-ion battery anodes. ACS Nano 4, 1443–1450. https://doi.org/10.1021/nn901409q.
Chen, Z., Fray, D.J., Farthing, T.W., 2000. Direct electrochemical reduction of titanium dioxide to titanium in molten calcium chloride. Nature 407, 361–364. https://doi.org/10.1038/35030069.
Cho, W.C., Kim, H.J., Lee, H.I., Seo, M.W., Ra, H.W., Yoon, S.J., Mun, T.Y., Kim, Y.K., Kim, J.H., Kim, B.H., Yoo, C.Y., Lee, J.G., Choi, J.W., 2016. 5L-scale magnesio-milling reduction of nanostructured SiO_2 for high capacity silicon anodes in lithium-ion batteries. Nano Lett. 16, 7261–7269. https://doi.org/10.1021/acs.nanolett.6b03762.
Chockla, A.M., Harris, J.T., Akhavan, V.A., Bogart, T.D., Holmberg, V.C., Steinhagen, C., Mullins, C.B., Stevenson, K.J., Korgel, B.A., 2011. Silicon nanowire fabric as a lithium ion battery electrode material. J. Am. Chem. Soc. 133, 20914–20921. https://doi.org/10.1021/ja208232h.
Choi, M., Kim, J.C., Kim, D.W., 2018. Waste windshield-derived silicon/carbon nanocomposites as high-performance lithium-ion battery anodes. Sci. Rep. 8, 960. https://doi.org/10.1038/s41598-018-19529-1.
Cui, J., Cui, Y., Li, S., Sun, H., Wen, Z., Sun, J., 2016. Microsized porous SiO_x@C composites synthesized through aluminothermic reduction from rice husks and used as anode for lithium-ion batteries. ACS App. Mater. Interfaces. 8 (454), 30239–30247. https://doi.org/10.1021/acsami.6b10260.
Ehrlich, H., Demadis, K.D., Pokrovsky, O.S., Koutsoukos, P.G., 2010. Modern views on desilicification: biosilica and abiotic silica dissolution in natural and artificial environments. Chem. Rev. 110, 4656–4689. https://doi.org/10.1021/cr900334y.
Fang, S., Wang, H., Yang, J., Lu, S., Yu, B., Wang, J., Zhao, C., 2015. Electrochemical preparation of silicon nanowires from porous NiO/SiO_2 blocks in molten $CaCl_2$. Mater. Lett. 160, 1–4. https://doi.org/10.1016/j.matlet.2015.07.082.
FAO, 2018. Food and Agriculture Organization (FAO) of the United Nations.
Fray, D., Schwandt, C., 2017. Aspects of the application of electrochemistry to the extraction of titanium and its applications. Mater. Trans. 58, 306–312. https://doi.org/10.2320/matertrans.MK201619.
Gauthier, M., Mazouzi, D., Reyter, D., Lestriez, B., Moreau, P., Guyomard, D., Roué, L., 2013. A low-cost and high performance ball-milled Si-based negative electrode for high-energy Li-ion batteries. Energy Environ. Sci. 6, 2145–2155. https://doi.org/10.1039/c3ee41318g.
Ghosh, A.K., Ahmed, S., Mollah, M.Y.A., 2013. Synthesis and characterization of zeolite NaY using local rice husk as a source of silica and removal of Cr(VI) from wastewater by zeolite. Bangladesh J. Sci. Ind. Res. 48, 81–88. https://doi.org/10.3329/bjsir.v48i2.15737.
Ji, H.S., Ryu, H.Y., Jeong, S.M., Cho, S.W., 2013. Fast electrochemical synthesis of $NdNi_5$ hydrogen storage alloy in molten salt. Chem. Lett. 42, 1182–1184. https://doi.org/10.1246/cl.130538.
Kasavajjula, U., Wang, C., Appleby, A.J., 2007. Nano- and bulk-silicon-based insertion anodes for lithium-ion secondary cells. J. Power Sources 163, 1003–1039. https://doi.org/10.1016/j.jpowsour.2006.09.084.
Kim, J.B., Lee, H.Y., Lee, K.S., Lim, S.H., Lee, S.M., 2003. Fe/Si multi-layer thin film anodes for lithium rechargeable thin film batteries. Electrochem. Commun. 5, 544–548. https://doi.org/10.1016/S1388-2481(03)00120-6.
Kim, H., Seo, M., Park, M.H., Cho, J., 2010. A critical size of silicon nano-anodes for lithium rechargeable batteries. Angew. Chem. Int. Ed. 49, 2146–2149. https://doi.org/10.1002/anie.200906287.
Kumproa, K., Singhykaew, S., Nuntiya, A., 2012. Effects of reaction time and hydrochloric acid concentration on acid hydrolysis of rice husk by reflux method. Adv. Mater. Res. 550–553, 592–597. https://doi.org/10.4028/www.scientific.net/AMR.550-553.592.
Lee, M.W., Choi, E.Y., Jeon, S.C., Lee, J., Park, S.B., Paek, S., Simpson, M.F., Jeong, S.M., 2016. Enhanced electrochemical reduction of rare earth oxides in simulated oxide fuel via co-reduction of NiO in Li_2O–LiCl salt. Electrochem. Commun. 72, 23–26. https://doi.org/10.1016/j.elecom.2016.08.021.
Liu, G., Xun, S., Vukmirovic, N., Song, X., Olalde-Velasco, P., Zheng, H., Battaglia, V.S., Wang, L., Yang, W., 2011. Polymers with tailored electronic structure for high capacity lithium battery electrodes. Adv. Mater. 23, 4679–4683. https://doi.org/10.1002/adma.201102421.
Liu, N., Wu, H., McDowell, M.T., Yao, Y., Wang, C., Cui, Y., 2012. A yolk-shell design for stabilized and scalable Li-ion battery alloy anodes. Nano Lett. 12, 3315–3321. https://doi.org/10.1021/nl3014814.
Liu, N., Huo, K., McDowell, M.T., Zhao, J., Cui, Y., 2013. Rice husks as a sustainable source of nanostructured silicon for high performance Li-ion battery anodes. Sci. Rep. 3 (1), 1–7. https://doi.org/10.1038/srep01919.
Luo, J., Zhao, X., Wu, J., Jang, H.D., Kung, H.H., Huang, J., 2012. Crumpled graphene-encapsulated Si nanoparticles for lithium ion battery anodes. J. Phys. Chem. Lett. 3, 1824–1829. https://doi.org/10.1021/jz3006892.
Luo, W., Chen, X., Xia, Y., Chen, M., Wang, L., Wang, Q., Li, W., Yang, J., 2017. Surface and interface engineering of silicon-based anode materials for lithium-ion batteries. Adv. Energy Mater. 7, 1701083. https://doi.org/10.1002/aenm.201701083.
Mohandas, K.S., Fray, D.J., 2004. FFC Cambridge process and removal of oxygen from metal-oxygen system by molten salt electrolysis: an overview. Trans. Indian Inst. Met. 57, 579–592.
Nguyen, H.T., Yao, F., Zamfir, M.R., Biswas, C., So, K.P., Lee, Y.H., Kim, S.M., Cha, S.N., Kim, J.M., Probat, C., 2011. Highly interconnected Si nanowires for improved stability Li-ion battery anodes. Adv. Energy Mater. 1, 1154–1161. https://doi.org/10.1002/aenm.201100259.
Nohira, T., Yasuda, K., Ito, Y., 2003. Pinpoint and bulk electrochemical reduction of insulating silicon dioxide to silicon. Nat. Mater. 2, 397–401. https://doi.org/10.1038/nmat900.
Park, M.H., Kim, M.G., Joo, J., Kim, K., Kim, J., Ahn, S., Cui, Y., Cho, J., 2009. Silicon nanotube battery anodes. Nano Lett. 9, 3844–3847. https://doi.org/10.1021/nl902058c.
Real, C., Alcala, M.D., Criado, J.M., 1996. Preparation of silica from rice husks. J. Am. Ceram. Soc. 79, 2012–2016. https://doi.org/10.1111/j.1151-2916.1996.tb08931.x.
Shah, A., Torres, P., Tscharner, R., Wyrsch, N., Keppner, H., 1999. Photovoltaic technology: the case for thin-film solar cells. Science 285, 692–698. https://doi.org/10.1126/science.285.5428.692.
Shen, Y., 2017. Rice husk silica derived nanomaterials for sustainable applications. Renew. Sustain. Energy Rev. 80, 453–466. https://doi.org/10.1016/j.rser.2017.05.115.
Wu, H., Cui, Y., 2012. Designing nanostructured Si anodes for high energy lithium ion batteries. Nano Today 7, 414–429. https://doi.org/10.1016/j.nantod.2012.08.004.

Xiao, W., Jin, X., Denf, Y., Wang, D., Hu, X., Chen, G.Z., 2006. Electrochemically driven three-phase interlines into insulator compounds: electroreduction of solid SiO_2 in molten $CaCl_2$. ChemPhysChem 7, 1750–1758. https://doi.org/10.1002/cphc.200600149.

Xu, C., Lindgren, F., Philippe, B., Gorgoi, M., Björefors, F., Edström, K., Gustafsson, T., 2015. Improved performance of the silicon anode for Li-ion batteries: understanding the surface modification mechanism of fluoroethylene carbonate as an effective electrolyte additive. Chem. Mater. 27, 2591–2599. https://doi.org/10.1021/acs.chemmater.5b00339.

Yasuda, K., Nohira, T., Amezawa, K., Ogata, Y.H., Ito, Y., 2005a. Mechanism of direct electrolytic reduction of solid SiO_2 to Si in molten $CaCl_2$. J. Electrochem. Soc. 152, D69–D74. https://doi.org/10.1149/1.1864453.

Yasuda, K., Nohira, T., Ito, Y., 2005b. Effect of electrolysis potential on reduction of solid silicon dioxide in molten $CaCl_2$. J. Phys. Chem. Solids 66, 443–447. https://doi.org/10.1016/j.jpcs.2004.06.037.

Zhou, S., Liu, X., Wang, D., 2010. Si/$TiSi_2$ heteronanostructures as high-capacity anode material for Li ion batteries. Nano Lett. 10, 860–863. https://doi.org/10.1021/nl903345f.